Shap. Mem. Superelasticity
https://doi.org/10.1007/s40830-023-00426-0

REVIEW

Superelasticity Induced by a Strain Gradient

Yang Yang[1] · Jun Sun[1] · Xiangdong Ding[1]

Received: 7 October 2022 / Revised: 10 January 2023 / Accepted: 1 February 2023

Abstract Superelasticity in bulk is known to originate from thermal-elastic martensitic transformation in shape memory alloys. The driving force arises from the volume free energy difference between the martensite and the parent phase. Here we review the observations of this novel superelastic behavior in various non-transformed systems driven by the nonuniform strain. We present several cases of shape recovery upon bending or torsion in metallic and non-metallic materials at small scale, such as α-Fe whisker, twinned CuAlNi martensite and $BaTiO_3$ membrane. The mechanism(s) of shape recovery were revealed by molecular dynamics simulations. The strain gradient could induce the formation of the nontypical interfaces, which could store a high interfacial energy to drive the deformed sample to recover to its original shape. The present paper provides insight on the origin of novel superelasticity induced by strain gradient.

Keywords Superelasticity · Strain gradient · Interfaces · Molecular dynamics

Introduction

Superelasticity is originally a characteristic property of shape memory alloys that have been studied for several decades. The accomplishment of superelasticity is associated with martensite transformation in conventional shape memory alloys [1]. The driving force arises from the free energy difference between the martensite and the parent phase [1–4]. These smart alloys have various applications in functional devices, such as sensors and actuators [1, 2, 5]. However, the superelasticity and shape memory effect breakdowns as the sample size reduces to ∼ 100 nm in some shape memory alloys [6, 7].

Many previous studies have shown that some non-transition systems could also exhibit the superelasticity when deforming under a nonuniform strain, such as bending or torsion [8–11]. For example, Brenner and Sears found that the metallic Cu and α-Fe whiskers could undergo shape recoverability after a large bending deformation [12, 13]. Otsuka et al. observed a novel bending superelasticity in a twinned CuAlNi martensite [14]. The molecular dynamics simulations were carried out probe the origin of shape recovery in these non-transition systems [15–18]. It was found that the non-conventional interfaces could form under the non-uniaxial loading. Although the movement of interface under a uniform stress field have been studied intensively, it is still unclear how these non-conventional interfaces are responsible for the shape recovery.

In this paper, we review the novel superelasticity induced by the gradient strain in several metallic and nonmetallic materials. The origin for shape recovery is closely related to the formation of nonconventional interface, significantly distinct from the martensitic transformation in traditional shape memory alloys. The

This invited article is part of a special issue of *Shape Memory and Superelasticity* honoring Professor Kazuhiro Otsuka for his 50 years of research on shape memory alloys and his 85th birthday. The special issue was organized by Dr. Xiaobing Ren, National Institute for Materials Science; Prof. Antoni Planes, University of Barcelona; and Dr. Avadh Saxena, Los Alamos National Lab.

✉ Xiangdong Ding
dingxd@mail.xjtu.edu.cn

[1] State Key Laboratory for Mechanical Behavior of Materials, Xi'an Jiaotong University, Xi'an 710049, China

Published online: 01 March 2023

nonconventional interfaces possess a high interfacial energy, providing the main driving force for the shape recovery. These observations extend the family of superelastic materials.

Shape Recovery Upon Bending Deformation in Non-Twinned Metallic Systems

Superelasticity Under Bending in Whiskers

It has been discovered that metallic whiskers can perform larger recoverable deformation in bending as early as 1950s [19]. For example, Herring and Galt first reported the bending behavior of tin whiskers in 1952 [19]. The maximum recoverable strain could reach 2–3 percent in tin whiskers with a diameter of several micrometers, far beyond the elastic limit for the bulk counterpart (Fig. 1a). The sharp bending preferred at a special angle, as shown in Fig. 1b. Sears et al. also reported a large recoverable bending in iron whiskers (Fig. 1c) [12]. A smooth bending could induce a full recovery from a strain of $1.4 \pm 0.1\%$, while a maximum strain of $12 \pm 2\%$ could be achieved for the sharp bending. The reversible dislocation movement, associated with the formation of small-angle grain boundaries, is assumed to account for the unique behavior. In addition, Brenner and Morelock reported that a bent Cu whisker recovers back to the straight shape after heating (Fig. 1d–g), similar with the shape memory effect [13]. However, no phase transformation occurs upon shape recovery.

Superelasticity Under Bending in α-Fe Nanowires

Molecular dynamics simulations have been applied to study the bending deformation in the α-Fe nanowires [16]. The interatomic interaction was described by an embedded atom method (EAM) developed by Mendelev et al. [20, 21]. Several atomic layers at both ends of the nanowire are set to be rigid as loading grips. Bending is induced by tilting the loading grips. The tilt was increased stepwise by $\Delta\theta = 1°$, where θ is the bending angle defined as half of the inclination angle of the two fixed surface layers against each other. Unloading was performed in a similar way by reducing the tilt angle. For each loading/unloading step, the sample was relaxed at 300 K for 0.1 ns using a Nosé-Hoover thermostat [22, 23]. All the simulations were performed using LAMMPS code [24]. The atomic configurations were displayed by AtomEye [25].

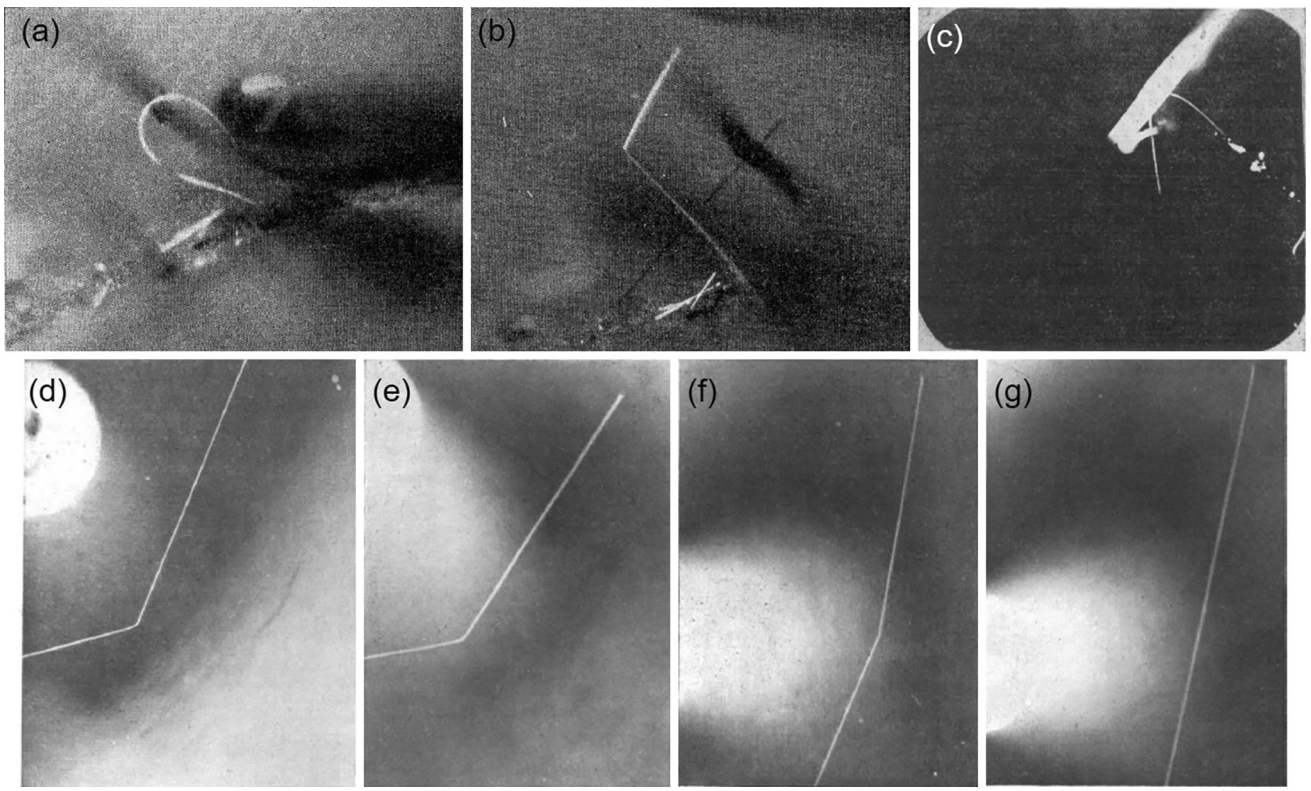

Fig. 1 **a** Bending of tin whisker with a radius of curvature of 9 mm [19]. **b** Same tin whisker with (**a**) after removal of constrain probe [19]. **c** Iron whisker with bending deformation exceeds elastic limit [12]. **d–g** Time sequence of recovery of a Cu whisker at 1015 °C: (**d**) 0 s, (**e**) 600 s, (**f**) 1460 s, and (**g**) 2400 s [13]

For BCC metallic nanowires, the common ⟨111⟩ /{112} type twinning is usually generated under the uniaxial deformation [26]. Here it was observed that the nonconventional {110} interfaces forms when the [100]-oriented α-Fe nanowires undergo bending [16]. Figure 2a shows a typical snapshot of the {110} interface in a side view at $\theta = 26°$. This nonconventional interface is formed by stacking a series of adjacent conventional⟨111⟩/{112} twin boundaries. Figure 2b–e show the atomic arrangement of each plane from the inside to the top surfaces in a top view. The {110} interface stems from the accumulation of individual⟨111⟩/{112} twin boundaries. The gradient strain field makes the thicknesses of the local⟨111⟩/{112} twin in each layer to decrease from the top layer downwards. Consequently, the local⟨111⟩/{112} "twins" construct the whole interface lying in a nonconventional {110} plane.

The α-Fe nanowire exhibits a much larger recoverable strain ($\theta = 80°$) with the aid of this {110} interface, as shown in Fig. 2f. The driving force for this novel superelasticity was further probed. It was found that the {110} interface has a higher interfacial energy (Fig. 2g). The release of this interfacial energy upon unloading can drive the bent nanowire to recover back. This is different from the superelasticity upon the uniform stress like tension, where the surface energy difference provides the driving force for shape recovery in metallic nanowires [26, 27].

The novel superelasticity upon bending is also confirmed by experiments. Figure 3a shows the transmission electron microscopy (TEM) images of the kinked twin boundaries in a bent tungsten nanowire [28]. The morphology of non-uniform stress induced deformation twinning is significantly distinct from that of traditional twinning under a uniaxial loading. It was found that a deformation band formed in this W nanowire, which thickened gradually with increasing strain. The formation of this deformation band also results in a kinked morphology [28]. The thickening of deformation band is completed by a layer-by-layer deformation twinning, keeping accordance with the atomistic simulations above [16]. In addition, an unstable twin structure with inclined twin boundary was observed in tungsten nanowires (Fig. 3b) [29]. The Moiré fringes in the TEM images indicate that the twin thickness could be different [29],

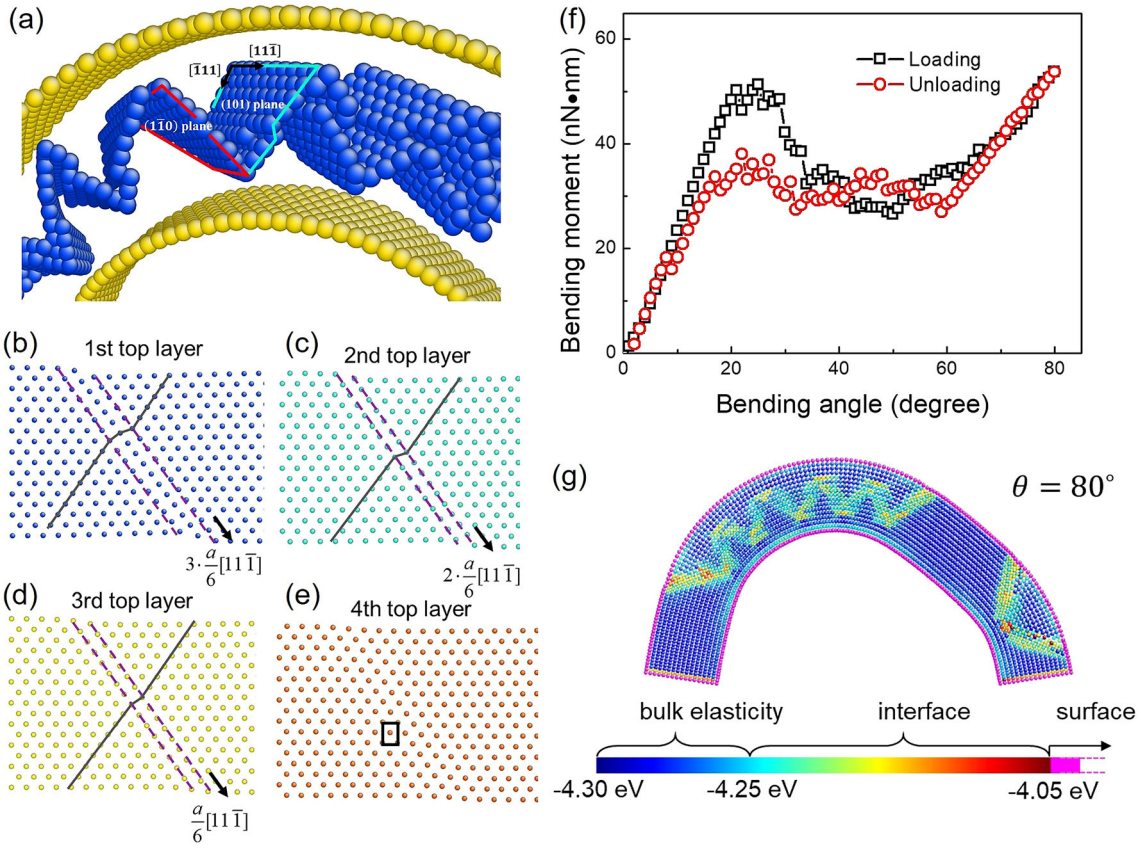

Fig. 2 **a** Snapshot of a {110} interface under bending in [100]-oriented single crystal α-Fe nanowire [16]. The morphology of the {110} interface is typically W-shaped. **b–e** Atomic images for each top single layer from inside to the top of the nanowire. **f** The variation of bending moment as a function of bending angle in α-Fe nanowire. **g** Distribution of potential energy in a bent nanowire at $\theta = 80°$. The colors are coded according to potential energy for each atom (Color figure online)

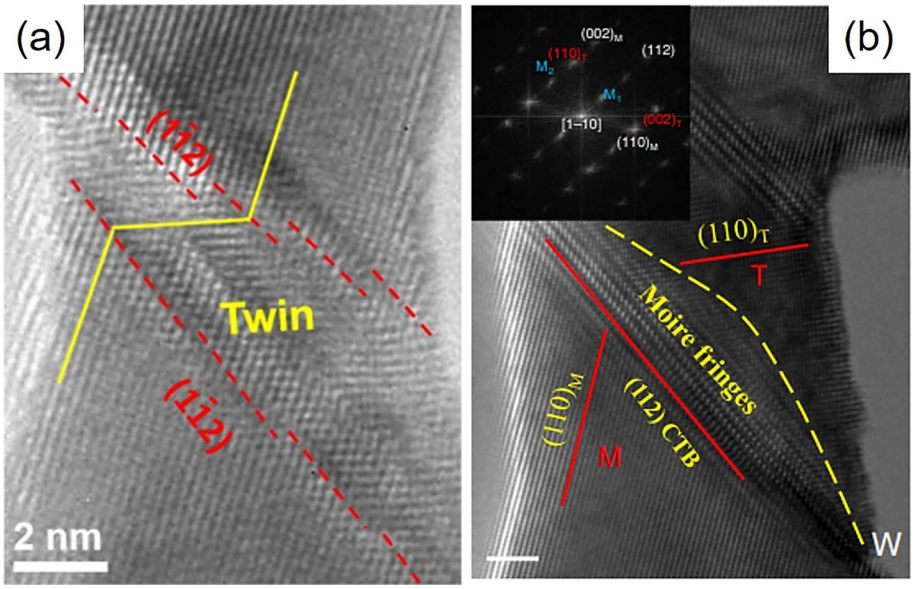

Fig. 3 **a** Zoomed-in image of the deformation twinning under non-uniaxial deformation in a W nanowire [28]. **b** Deformation twin with the Moiré fringe near coherent twin boundary in a W nanocrystal [29]

which might correlate with the formation of nonconventional {110} interface.

Shape Recovery Upon Bending Deformation in Twinned Metallic Systems

Superelasticity in a CuAlNi Twinned Martensite

Otsuka et al. observed a bending superelasticity in a twinned CuAlNi martensite [14]. Figure 4a shows that CuAlNi martensite could undergo a reversible bending deformation, while it cannot exhibit the recovery ability upon uniaxial tension (Fig. 4b) or compression (Fig. 4c). Tension and compression could only induced domain switching via the movement of twin, which is usually irreversible in martensite. On the contrary, bending could generate a strain gradient field. The parallel pre-existing twins evolve into the wedged shape upon bending. The deformed triangle regimes could recover back upon unloading (Fig. 4d). The gradient stress field in bending induces the movement of the twin boundaries along opposite directions from the top to the bottom surfaces (Fig. 4d). This induces the accumulation of partial dislocations with the same Burgers vector at the deformed interfaces. The strong repulsive force among these partials is assumed to drive the bent sample to return its original shape.

The mechanism for the superelasticity discovered in the CuAlNi twinned martensite is obviously distinct from that in shape memory alloys. On the one hand, no martensitic phase transformation occurs upon bending deformation in this CuAlNi martensite. On the other hand, although the superelasticity is observed in a martensite, the recovery can only be achieved in bending, unlike the rubber-like behavior [30].

Superelasticity in a Multi-Twinned α-Fe Nanowire

Molecular dynamics simulations were also performed to investigate the superelasticity upon bending in multi-twinned α-Fe nanowires [15]. A series of parallel⟨111⟩ / {112} twin boundaries have been introduced in the α-Fe nanowire (Fig. 5a), in analogy to the topological structures observed in CuAlNi experimentally [14]. Figure 5b shows the atomic configuration of two variants. The maximum tensile stress σ_{max} and the maximum tensile strain ε_{max} on the top surface were used to characterize the bending properties. ε_{max} is calculated as the bending angle θ divided by the aspect ratio of the sample as $\varepsilon_{max} = \theta d/L$. The maximum tensile stress is $\sigma_{max} = -Md/(2I)$, where M is the bending moment, I is the moment of inertia, and $d/2$ is the distance from the neutral line to the surface of the nanowire.

Figure 5c shows the variation of σ_{max} as a function of ε_{max} upon bending. The twinned nanowire yields with σ_{max} = 2.2 GPa at ε_{max} = ~ 2%. A strong strain hardening after yielding is observed until ε_{max} = ~ 7%. A full recovery strain ε_{max} = ~ 7% was observed upon unloading, which is much larger than the maximum recoverable strain of ~ 0.05% in bulk α-Fe [31] and ~ 1.4% in α-Fe whiskers [12]. Figure 5d–f shows typical atomic configurations of reversible twin boundary movement upon loading and unloading. The boundary motion is completed via the glide of 1/6⟨111⟩ partial dislocations. Staring from perfect $(2\bar{1}\bar{1})$ twin planes at $\theta = 0°$ (Fig. 5d), twin

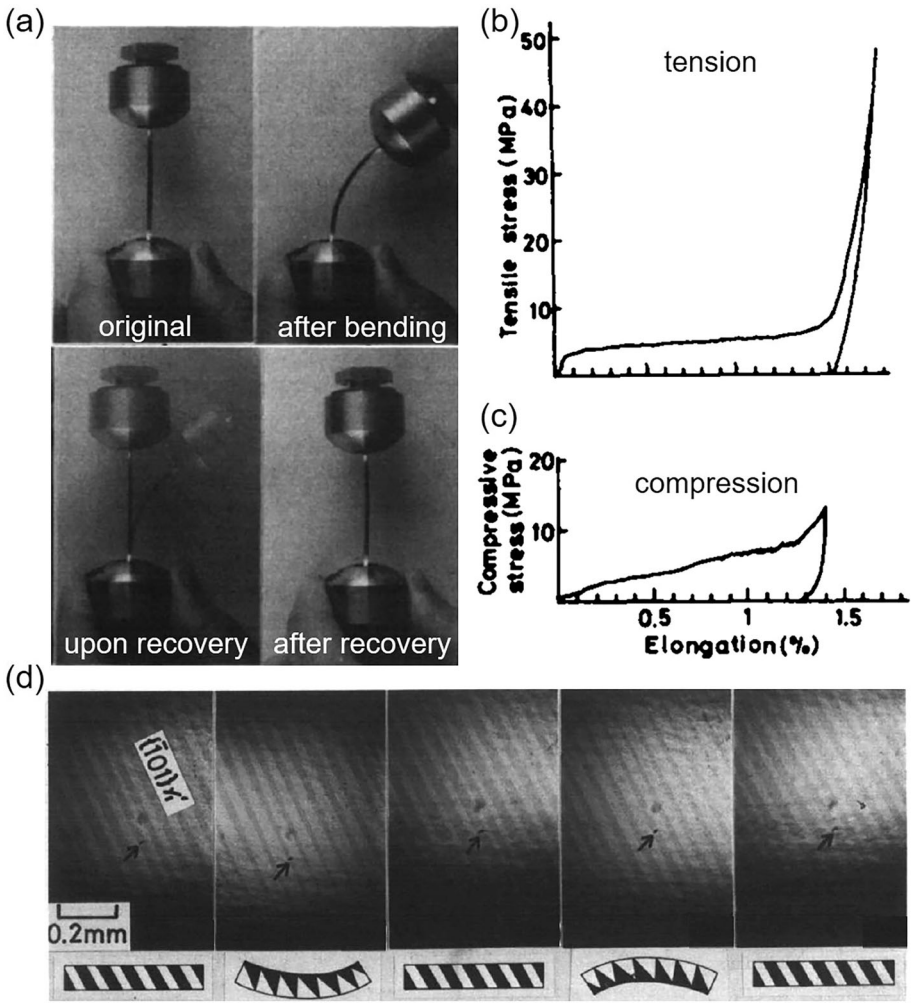

Fig. 4 **a** Bending superelasticity in a twinned Cu–Al–Ni martensite [14]. Stress–strain curves for **b** tension and **c** compression tests for this Cu–Al–Ni martensite. **d** Microstructural changes associated with bending

boundaries become curved upon bending (Fig. 5e). There are many partial dislocations accumulating at the twin boundaries. After unloading, the bent boundaries become flat, leading to a full recovery (Fig. 5f).

The accomplishment of superelasticity is close related to the deformed interfaces, which store a high interfacial energy and provide the main driving force for shape recovery. However, the recoverability becomes weakened once the full dislocation nucleation and detwinning occur. It was found that full dislocations prefer to nucleate once the twin boundary density is very low, while detwinning occurs once the twin boundary density is very high. The shape recoverability might be manipulated by tuning the twin boundary density. Here the twin boundary density is characterized by the ratio η of wire diameter d to twin spacing s. Figure 5g shows the size dependence of the maximum recoverable strain $\varepsilon_{max}^{recovery}$ with η. The experimental value of $\varepsilon_{max}^{recovery}$ of bulk Cu–Al–Ni [14] is also marked (red star in Fig. 5g). This parameter η can be extended to capture this experimental value quite well ($\eta \sim 60$). The size-dependent recoverability agrees well with the stored partial dislocation density (Fig. 5h), indicating the important role that the stored partials play in achieving superelasticity. The simulation results implies that bending-induced superelasticity of twinned sample could exist in a wide range of length scale.

Superelastic Ferroelectric Single-Crystal $BaTiO_3$ Membrane

Bending superelasticity is also observed in a ferroelectric ceramic $BaTiO_3$ (BTO) [18]. Figure 6a shows the bending tests on BTO nanobelts with a thickness of 60 nm. One nano-manipulator tip is used to hold the BTO nanobelt (120 nm), and another nanomanipulator tip is used to push the BTO nanobelt to bend. A maximum strain of $\sim$ 10% in the BTO nanobelt is achieved without any fracture, demonstrating excellent flexibility in this BTO membrane. The bent BTO membrane could almost revert back to the original shape after removing the external load.

Figures 6b–g show the atomistic simulations on the microstructure evolution under mechanical bending in the

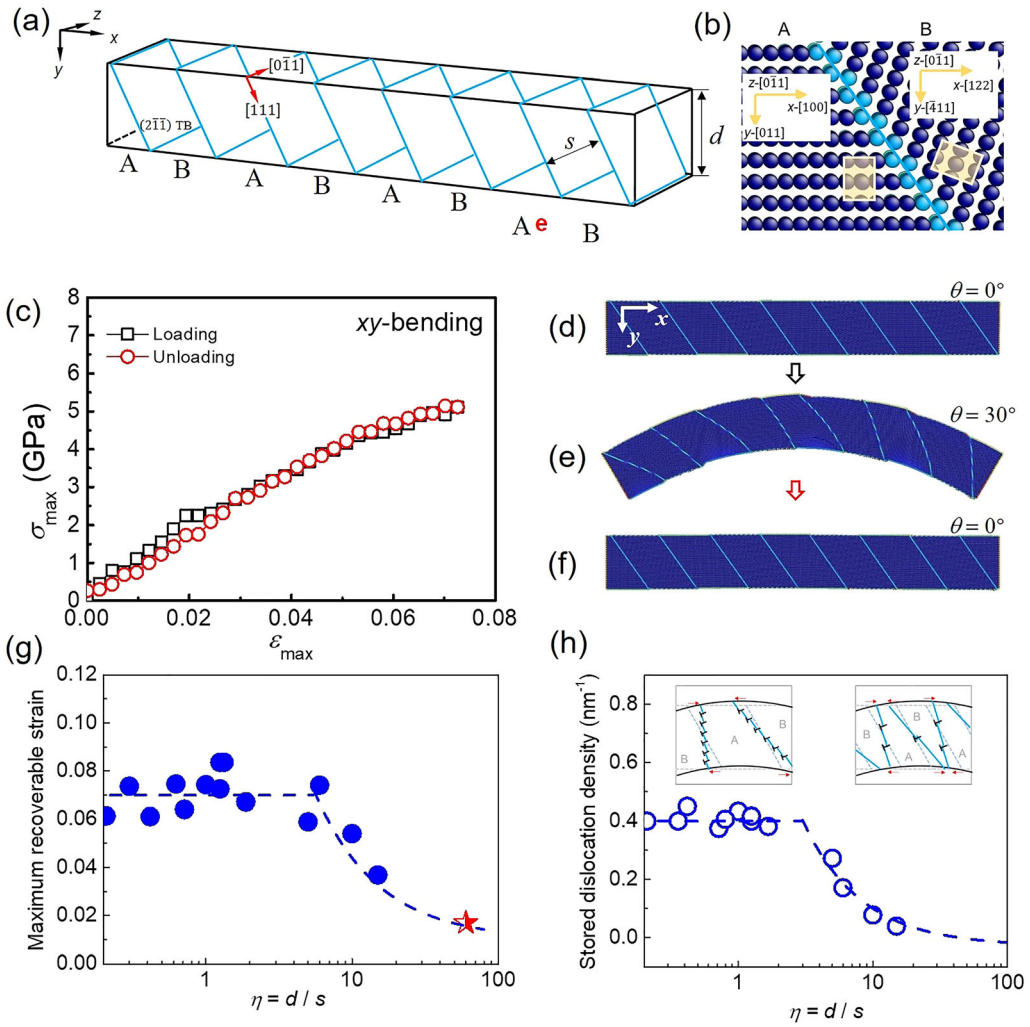

Fig. 5 Pseudoelasticity in twinned α-Fe nanowires under bending [15]. **a** Schematic illustration of the α-Fe nanowire seeded with⟨111⟩/{112} twin boundaries. **b** The sample contains two variants. **c** Maximum tensile stress σ_{max} vs maximum tensile strain ε_{max} curves for the *xy*-bending. **d–f** Typical atomic images upon loading and unloading for the *xy*-bending. **g** The variation of maximum recoverable strain and (**h**) density of stored partial dislocations per TB as a function of η, which is a ratio of wire diameter *d* to twin spacing *s*. The dashed lines are guide for eyes. The insets illustrate the accumulation of partial dislocations at the interfaces schematically in the two distinct regimes

BTO membranes at 300 K [18]. Figure 6b shows the variation of bending moment as a function of bending angle upon loading and unloading, indicating a typical superelastic behavior. The total recoverable strain could reach ∼ 10%, close to the experimental value. Figure 6c shows the original dipole configurations at the atomic scale. Before loading, the lattices are identified as *c* nanodomains with polarization either upward (red arrows) or downward (blue arrows). Upon bending, the vertical dipoles in the tensile regions began to rotate locally at a smaller bending angle (Fig. 6d). Further bending promotes the local nanodomains to grow up into a nanodomain with left or right polarizations (black or green arrows, *a* domains) (Fig. 6e). As the considerable bending angle is applied, one oriented a nanodomain grew to cover the whole free surface, forming a 180° domain boundary with a few steps (Fig. 6f). It was observed that dipoles rotate continuously in a transition zone connecting *a* and *c* domains (Fig. 6g). The formation of such a continuous transition zone could largely eliminate the mismatch stress in the coexisting *c* and *a* nanodomains at high strain, avoiding the mechanical failure by the sharp domain switching [18].

Superelasticity Under Torsion in Twinned Metallic Nanowires

Besides bending, torsion is another typical deformation mode that generates nonuniform strain, i.e., shear strain gradient. The superelasticity is also observed in torsion in

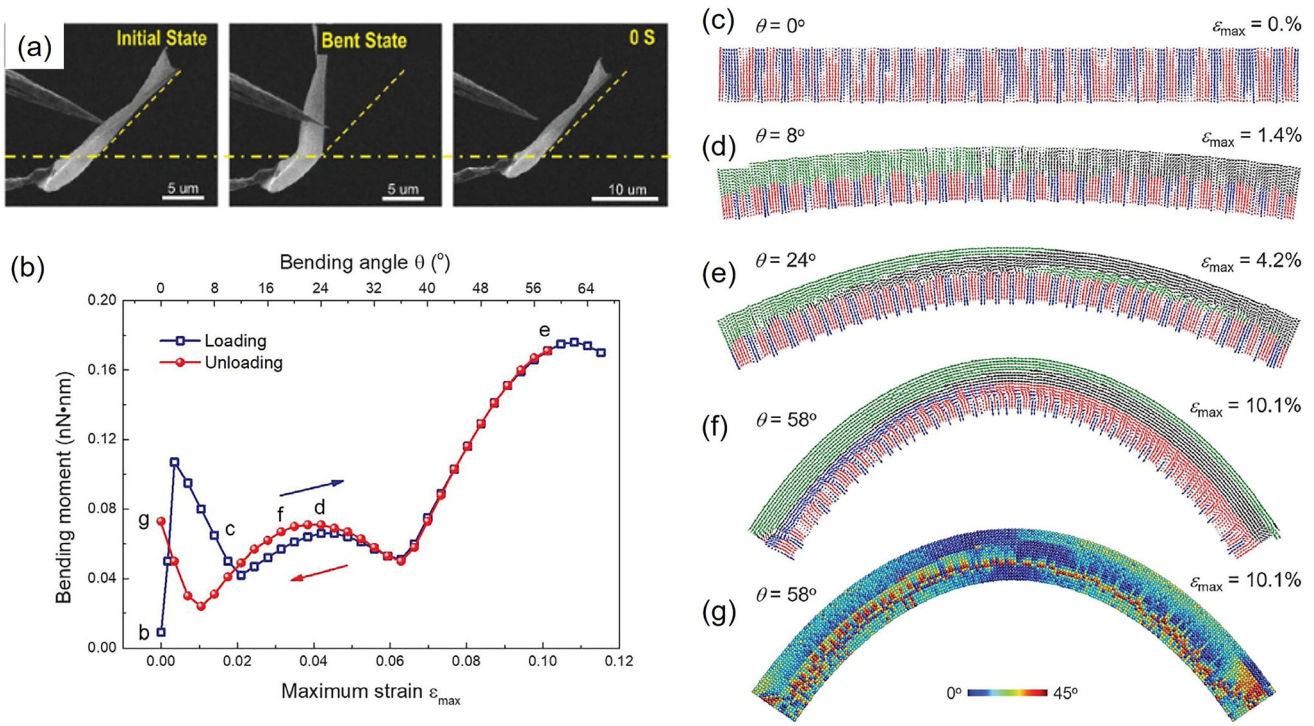

Fig. 6 Superelasticity mediated with continuous electric dipole rotation in a $BaTiO_3$ (BTO) ferroelectric single-crystal membrane [18]. **a** Scanning electron microscope images of the recovery process after the different bending states for a BTO nanobelt. **b** Variation of bending moment with bending angle θ (and maximum strain ε_{max}) upon loading and unloading with sample width of 8 nm. **c–f** Typical snapshots of dipole configurations at different bending angles. The black and green arrows represent the dipoles with *x* components left and right, respectively, in the tensile region. The red and blue arrows represent the dipoles with y components up and down, respectively, in the compressive region. Dipole displacements are amplified by a factor of 50 for clarity. **g** Spatial distribution of angle deviation η with respect to the *a* or *c* nanodomain at $\theta = 58°$. η characterizes the deviation of dipole rotation with respect to the a or c domains by using the parameter $\eta = \pi/4 - |\varphi - (n*\pi/2 + \pi/4)|$ for $\varphi \in [n*\pi/2, (n + 1)*\pi/2]$, where φ is the rotation angle of polarization concerning the central axis in each unit cell and *n* runs from 0 to 3 (Color figure online)

the twinned α-Fe nanowires [17, 32]. Here two kinds of pre-existing twin patterns were introduced into α-Fe nanowires, i.e., the parallel twin boundaries with the normal direction along the wire axis in a ⟨112⟩ -oriented nanowire and the six-fold twinned structure in a⟨111⟩-oriented nanowire. Figure 7a shows the variation of torque as a function of torsion angle in a multi-twinned α-Fe nanowire with a series of parallel twin boundaries. Twisting induces the transformation of normal {112} twin boundary to nonconventional {110} interfaces (Fig. 7b), leading to a good shape recovery (blue line in Fig. 7a). However, once the torsion angle exceeds a critical value, structural instability occurs in twin boundaries or interfaces (Fig. 7c), inducing irreversible deformation (red line in Fig. 7a).

Similar superelasticity is also observed in a six-fold twinned α-Fe nanowire upon torsion, as shown in Fig. 7d–h. Compared with the original structure (Fig. 7d), smaller torsion angle only induces structural evolution of twin boundaries (Fig. 7e), which can get full recovery after unloading (Fig. 7g). However, once the torsion angle is larger than the critical value, full dislocations nucleate. Shape recoverability then becomes weakened correspondingly (Fig. 7f and h) [33].

Summary

In this review, we summarized gradient strain induced superelasticity in both metallic and nonmetallic materials. Different from the classical superelasticity associated with martensitic transformation, the bending or torsion could promote the formation of nonconventional interfaces. The deformed nonconventional interface could store a high interfacial energy, providing the majority of driving force for the unique shape recovery. These studies could provide

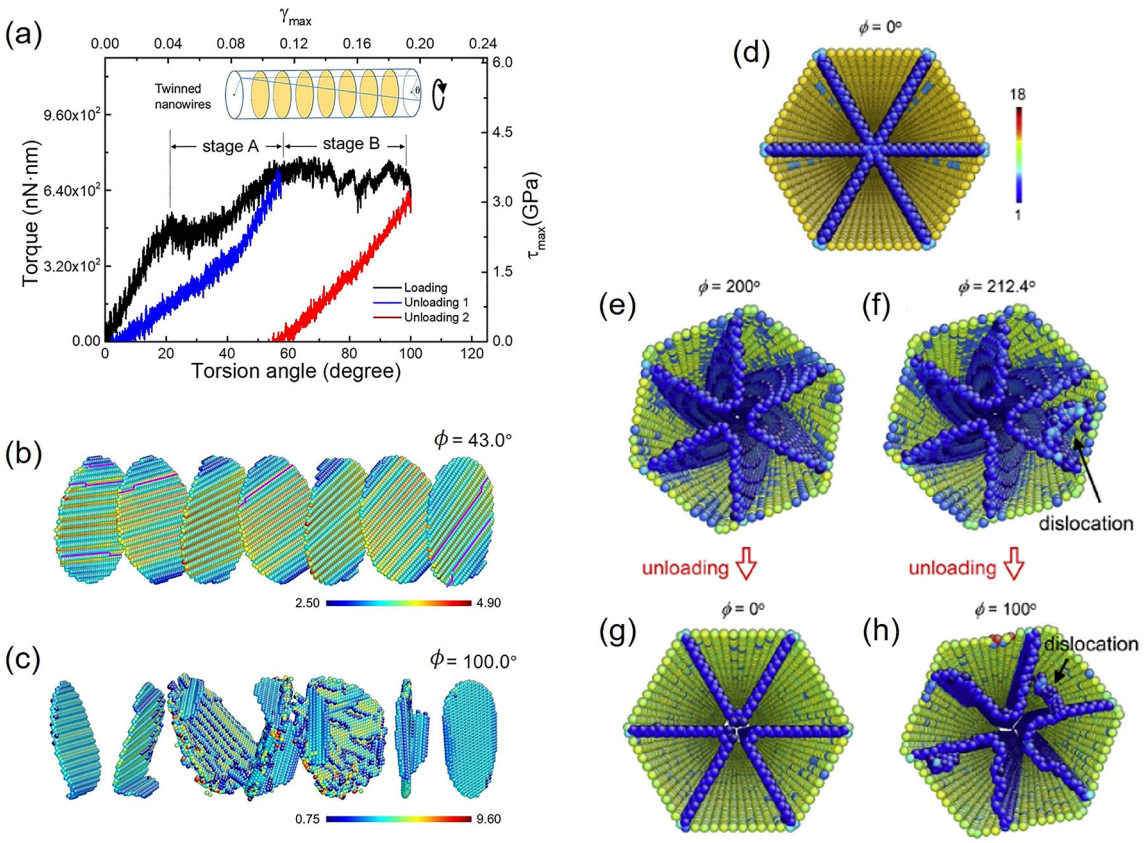

Fig. 7 **a** Variation of torque (and maximum shear stress τ_{max}) with the applied torsion angle (and maximum shear strain γ_{max}) for [112]-oriented twinned nanowires [17]. Two stages of plasticity are distinguished according to the recoverability. Atomic configurations of twin boundaries at (**b**) φ = 43° and (**c**) φ = 100.0° [17]. **d**–**h** Typical images of plastic deformation of six-fold twinned nanowires [32]. **d** The initial configuration with three equivalent preexisting twin boundaries. **e** The twin boundaries are severely twisted. **f** Full dislocations are generated. **g** Unloading at state φ = 200°. **h** Unloading at state φ = 212.4°. The color is shown according to the centro-symmetry parameter [34] (Color figure online)

insights on the origin of recoverable deformation driven by the nonuniform strain in non-transition systems.

Acknowledgements This work was supported by the National Natural Science Foundation of China (12104355 and 51320105014), and the 111 project 2.0 (BP2018008).

References

1. Otsuka K, Wayman CM, Nakai K, Sakamoto H, Shimizu K (1976) Superelasticity effects and stress-induced martensitic transformations in CuAlNi alloys. Acta Metall 24:207
2. Otsuka K, Ren X (2005) Physical metallurgy of Ti–Ni-based shape memory alloys. Prog Mater Sci 50:511
3. Planes A, Mañosa L (2001) Vibrational properties of shape-memory alloys. Solid State Physics 55:159
4. Ding X, Suzuki T, Ren X, Sun J, Otsuka K (2006) Precursors to stress-induced martensitic transformations and associated superelasticity: molecular dynamics simulations and an analytical theory. Phys Rev B 74:104111
5. Duerig TW, Pelton AR, Stöckel D (1996) The utility of superelasticity in medicine. Bio-Med Mater Eng 6:255
6. Waitz T, Antretter T, Fischer FD, Simha NK, Karnthaler H-P (2007) Size effects on the martensitic phase transformation of NiTi nanograins. J Mech Phys Solids 55:419
7. Liu L, Ding X, Sun J, Li S, Salje EKH (2016) Breakdown of shape memory effect in bent Cu–Al–Ni nanopillars: when twin boundaries become stacking faults. Nano Lett 16:194
8. Stan G, Krylyuk S, Davydov AV, Levin I, Cook RF (2012) Ultimate bending strength of Si nanowires. Nano Lett 12:2599
9. Tang L, Zhao Y, Liang N, Islamgaliev RK, Valiev RZ, Zhu YT (2016) Localized deformation via multiple twinning in a Mg–Gd–Y–Zr alloy processed by high-pressure torsion. Mater Sci Eng: A 677:68
10. Schönherr E, Winckler E (1976) Bending and straightening of GaP whiskers during their growth. J Cryst Growth 32:117
11. Chopra HD, Bailly C, Wuttig M (1996) Domain structures in bent In-22.5 at.% Tl polydomain crystals. Acta Materialia 44:747
12. Sears GW, Gatti A, Fullman RL (1954) Elastic properties of iron whiskers. Acta Metall 2:727
13. Brenner SS, Morelock CR (1956) The high-temperature recovery of deformed copper whiskers. Acta Metall 4:89
14. Otsuka K, Sakamoto H, Shimizu K (1977) A new type of pseudoelasticity in single variant twinned Martensites. Scr Metall 11:41
15. Yang Y, Li S, Ding X, Sun J (2021) Pseudoelasticity in twinned α-Fe nanowires under bending. Comput Mater Sci 188:110128

16. Yang Y, Li S, Ding X, Sun J, Salje EKH (2016) Interface driven pseudo-elasticity in α-Fe nanowires. Adv Func Mater 26:760
17. Yang Y, Li S, Ding X, Sun J, Weiss J, Salje EKH (2020) Twisting of pre-twinned α-Fe nanowires: from mild to wild avalanche dynamics. Acta Mater 195:50
18. Dong G, Li S, Yao M, Zhou Z, Zhang Y, Han X, Luo Z, Yao J, Peng B, Hu Z, Huang H, Jia T, Li GY, Ren W, Ye ZG, Ding X, Sun J, Nan CW, Chen L, Li J, Liu M (2019) Super-elastic ferroelectric single-crystal membrane with continuous electric dipole rotation. Science 366:475
19. Herring C, Galt JK (1952) Elastic and plastic properties of very small metal specimens. Phys Rev 85:1060
20. Mendelev MI, Han S, Srolovitz DJ, Ackland GJ, Sun D, Asta M (2003) Development of new interatomic potentials appropriate for crystalline and liquid iron. Phil Mag 83:3977
21. Daw MS, Baskes MI (1984) Embedded-atom method: derivation and application to impurities, surfaces, and other defects in metals. Phys Rev B 29:6443
22. Hoover WG (1985) Canonical dynamics: equilibrium phase-space distributions. Phys Rev A 31:1695
23. Nosé S (1984) A unified formulation of the constant temperature molecular dynamics methods. J Chem Phys 81:511
24. Plimpton S (1995) Fast parallel algorithms for short-range molecular dynamics. J Comput Phys 117:1
25. Li J (2003) AtomEye: an efficient atomistic configuration viewer. Modell Simul Mater Sci Eng 11:173
26. Li S, Ding X, Li J, Ren X, Sun J, Ma E (2010) High-efficiency mechanical energy storage and retrieval using interfaces in nanowires. Nano Lett 10:1774
27. Li S, Ding X, Deng J, Lookman T, Li J, Ren X, Sun J, Saxena A (2010) Superelasticity in bcc nanowires by a reversible twinning mechanism. Phys Rev B 82:205435
28. Wei S, Wang Q, Wei H, Wang J (2019) Bending-induced deformation twinning in body-centered cubic tungsten nanowires. Mater Res Lett 7:210
29. Wang X, Wang J, He Y, Wang C, Zhong L, Mao SX (2020) Unstable twin in body-centered cubic tungsten nanocrystals. Nat Commun 11:1
30. Ren X, Otsuka K (1997) Origin of rubber-like behaviour in metal alloys. Nature 389:579
31. Howatson AM, Lund PG, Todd JD (1972) Engineering tables and data. Chapman and Hall, London
32. Li S, Salje EKH, Sun J, Ding X (2017) Large recovery of six-fold twinned nanowires of α-Fe. Acta Mater 125:296
33. Yang Y, Ding X, Sun J, Salje EKH (2021) Twisting of a pristine α-Fe nanowire: from wild dislocation avalanches to mild local amorphization. Nanomaterials 11:1602
34. Kelchner CL, Plimpton SJ, Hamilton JC (1998) Dislocation nucleation and defect structure during surface indentation. Phys Rev B 58:11085